Journal of Materials and Environmental Science
ISSN : 2028-2508
e-ISSN : 2737-890X
CODEN : JMESCN

J. Mater. Environ. Sci., 2023, Volume 14, Issue 04, Page 491-510

http://www.jmaterenvironsci.com

Study of Adsorption of Hydrogen Sulfide in Biogas with Musa Paradisicaca Activated Carbon using Full Factorial Design

Konan Remis GBANGBO[1,3*], Adjoumani Rodrigue KOUAKOU[2], Ahissan Donatien EHOUMAN[2], Benjamin YAO[1,4], Kopoin ADOUBY [1], Gonezie Vanessa-Edwige GOLI LOU[3], Zephirin GNABOA[3],**

[1] Laboratory of Industrial Processes and Synthesis of New Energies (LAPISEN), National Polytechnic Institute Felix Houphouet-Boigny (INP-HB) ; BP 1093 Yamoussoukro, Tel. (+225) 27 30 64 67 15 (Ivory Coast);
[2] Laboratory of Thermodynamics and Physical and Environmental Chemistry (LTPCM), UFR Applied Fundamental Sciences, Nangui Abrogoua University, Abidjan, Ivory Coast, B.P. 801 Abidjan 02, Tel. (+225) 27 20 30 42 00
[3] Hydraulics and Water Treatment Laboratory, National Polytechnic Institute Felix Houphouet-Boigny (INP-HB) ; BP 1093 Yamoussoukro, Tél. (+225) 27 30 64 67 15 (Côte d'Ivoire);
[4] African Centre of Excellence for the Valorisation of Waste into High Value Products (CEA-VALOPRO), World Bank Excellence Center, National Polytechnic Institute Felix Houphouet-Boigny (INP-HB); BP 1093 Yamoussoukro, Tél. (+225) 27 30 64 67 15 (Ivory Coast)
**Corresponding author, Email address: konanremis@gmail.com; gbangbo.konan19@inphb.ci*
***Corresponding author, Email address: adjoumanro@gmail.com;*

Received *16 Mar 2023,*
Revised *17 Apr 2023,*
Accepted *21 Apr 2023*

Keywords:
- ✓ *H_2S adsorption;*
- ✓ *Biogas;*
- ✓ *Activated Carbon;*
- ✓ *Musa Paradisiaca;*
- ✓ *Full factorial design*

Citation*: Gbangbo K. R., Kouakou A. R., Ehouman A. D., Yao B., Adouby K., Goli Lou G. V. E., Gnaboa Z. (2023) Study of Adsorption of Hydrogen Sulfide in Biogas with Musa Paradisicaca Activated Carbon using Full Factorial Design, J. Mater. Environ. Sci., 14(4), 491-510.*

Abstract: In this study, the simultaneous influence of different factors such as biogas flow rate, water content and iron oxide on H_2S adsorption from biogas with activated carbon (AC) developed from Musa Paradisiaca (MP) peels was demonstrated using full factorial design method. AC was activated at 500°C for 3 hours after basic impregnation with potassium hydroxide. The values of the studied parameters ranged from 0 to 25% and 1 to 3 $L.min^{-1}$ for water content and flow rate, respectively. The AC was functionalized or not with iron oxide (Fe_2O_3). Responses studied in the adsorption tests were saturation time and adsorption capacity. The results showed that water content and the presence of iron (Fe) nanoparticles positively affect the adsorption capacity and saturation time. Furthermore, an increase in the flow rate decreases the adsorption capacity and the saturation time. Moreover, three interactions were highlighted through the study of coefficients obtained from the full factorial design. First, water content and increasing flow rate act simultaneously to decrease the adsorption capacity of AC. Secondly, water content and Iron impregnation simultaneously act positively on the adsorption capacity. Finally, the interaction between flow rate and the presence of iron oxide was found to be insignificant. A first-degree mathematical model was used to describe the adsorption of H_2S on MP peels: the highest adsorption capacity of CA obtained under our experimental conditions is 9.86 $mgH_2S.g^{-1}$, with an addition of 25% water in the AC already impregnated with Fe. The biogas flow rate was 1 $L.min^{-1}$. The functionalized AC that gave the highest adsorption capacity had a micropore volume of 0.92 cm^3/g^{-1}, and a specific surface area of 76.18 m^2g^{-1}. The average pore diameter was 0.74 nm. This indicates that it contains micropores.

1. Introduction

The current global energy crisis is unprecedented. In March 2022, energy prices were more than four times higher than their lowest prices in April 2020 (World bank, 2022). This is the result of tensions in global markets that emerged in the wake of the recovery from the Covid-19 recession and were

amplified by the war in Ukraine beginning in early 2022 (Insee, 2022). Moreover, fossil fuels (oil, coal and natural gas), which represent 80% of the world's energy consumption, are at the origin of the worsening of our climate emergency (UNEP, 2022). Indeed, the last few months have been marked by record highs in climate indicators: this heralds a future of ferocious storms, floods, droughts, forest fires and scorching temperatures over large areas of the planet. This situation has led the Secretary General of the United Nations to state: "The world is burning, we need a renewable energy revolution" (Guterres, 2022). Among these renewable energies, we find biogas. It is a non-intermittent energy with multiple uses (Gasquet, 2021) produced from organic waste from industries, landfills and domestic waste via anaerobic processes (Sethupathi et al., 2017). Thus, biogas represents both an energy and environmental solution in the sense that its production results from a sustainable process established for the simultaneous generation of renewable energy and treatment of organic waste (Nyamukamba et al., 2022).

Biogas is composed of methane (CH_4), carbon dioxide (CO_2), water (H_2O), hydrogen sulfide (H_2S), and trace elements. H2S is a highly odorous, toxic, and corrosive compound (Abdirakhimov et al., 2022). At concentrations between 1,000 and 2,000 ppm, H_2S can cause coma and death within seconds after one or two inhalations (Nabais et al., 2011). At concentrations of 100 to 200 ppm, H2S can cause blurred vision and death after 1 to 8 hours of exposure (Nabais et al., 2011). In addition, dissolved H_2S with concentration up to 50 ppm causes fermentation inhibition as it is toxic to bacteria in bioreactor sludge (Yuan et al., 2019). At the environmental level, the combustion of H_2S forms sulfur dioxide (SO_2), leading to the formation of a highly corrosive gas and is a major source of acid rain (Awe et al., 2017). Therefore, the removal of H_2S from biogas is of critical importance, technically, environmentally and health-wise. For this purpose, there are several industrial methods of purification based on chemical, biological, or physical principles including biological desulfurization, chemical absorption, water scrubbing, membranes, and adsorption on adsorbent materials (Sawalha et al., 2020). Nevertheless, the complexity and costs associated with these treatment processes are a hindrance to their development (Fougerit, 2017), especially in developing countries. It is therefore essential to consider the treatment of H_2S from biogas with local, available and cheap materials. In this sense, several works have focused on the use of carbon as an adsorbent material for H_2S adsorption (Abdirakhimov et al., 2022, Choudhury and Lansing, 2021, Sawalha et al., 2020, Shang et al., 2016)

Several parameters influence the adsorption of H_2S from biogas onto activated carbon. Thus, the mechanisms of H_2S adsorption are a combination of different factors. Guofeng Shang (2016) showed that increasing the biochar production temperature (in the range of 100-500°C increases the adsorption capacity of H_2S. This finding was made on 3 different biochars from agricultural/forestry waste produced by pyrolysis. Furthermore, by impregnating the char with iron chloride, Choudhury and Lansing (2021) increased the adsorption capacity of maple wood biochar by a factor of 3.5. Additionally, Chemisorption with H_2S is strongly promoted by KOH impregnation and the presence of water also affects adsorption capacity of H_2S (Sitthikhankaew et al., 2014). Each of these different works focused on evaluating the effect of one factor on the mechanism of H_2S adsorption from biogas: studying the influence of parameters taken one by one on H_2S adsorption by activated carbon. This method consists in fixing a certain number of parameters and to make vary one of them and to note its influence on the adsorption. This approach does not make it possible to highlight the interactions between the different variables which act on the adsorption mechanism. This deficit has led researchers to contradict each other. For example, Choudhury and Lansing (2021) disputed the results of Shang et al., (2016) work that low pH and sulfuric acid formation on the surface of Activated Carbon would be the main reasons for its low

adsorption capacity. What would happen if the factors influencing the adsorption capacity of H_2S on activated carbon were varied simultaneously? Statistical tools are available to answer this question, including experimental designs, especially full factorial design. Recently, the adsorption capacity of banana peel biochar (BPB) and banana empty fruit bunch biochar (BEFBB) wastes for removing H_2S from biogas was investigated (Juntarachat and Onthong, 2022) but to the best of our knowledge, no study has investigated the use of experimental designs by simultaneously varying the parameters of flow rate, water content and Iron (Fe) nanoparticles impregnation to understand their simultaneous influence on H_2S adsorption from biogas. In addition, no study to our knowledge has investigated the use of Musa Paradisiaca (MP) peels as activated carbon for H_2S removal from biogas. This study focuses on the use of the design of experiments method, particularly full factorial designs to evaluate the interactions between water content, gas flow rate and impregnation of MP activated carbon with iron nanoparticles. This will allow the modelling of H_2S adsorption as a function of these three (03) factors. Finally, it will be established the optimal conditions to obtain the greatest capacity of H_2S adsorption by activated carbon of MP in our experimental conditions.

2. Materials and methods

2.1.Preparation of activated carbon

2.1.1. Choice of raw material

Musa Paradisiaca (plantain) plays an important role in the economy of rural areas in Ivory Coast. Its production, estimated at 1.5 million tons per year, makes Côte d'Ivoire the 8th largest producer in the world (Coffi et al., 2021). Plantain accounts for 20% of food production, occupying 3rd place behind yam and cassava, and 25% of all starchy foods consumed in Côte d'Ivoire (Coffi et al., 2021). The development of urban centers has led to an explosion in demand for plantain. It is thus a high value-added crop in the major cities. As the fleshy peel represents 30 to 40% of the weight of the fruit, it would be a shame not to recycle this organic material. In addition, it contains 20 to 30% fiber (cellulose, hemicellulose and lignin): it is therefore a suitable material for the production of activated carbon (Koné et al., 2021; Ngakou, 2019).

2.1.2. Synthesis of activated carbon

Musa Paradisiaca (MP) peels were collected from households and restaurants in Djahakro, a village not far from INP-HB (Institut National Polytechnique Félix Houphouët-Boigny of Yamoussoukro, Côte d'Ivoire). The peelings were then dried in the sun (**Figure 1**) for several days until they were sufficiently dry, and then ground to a diameter of between 800 µm and 3 mm. A 500 ppm potassium hydroxide (KOH) solution was prepared with distilled water as an activating agent. The shredded material was impregnated with the potassium hydroxide (KOH) solution at an impregnation ratio of 0.3 $g.mL^{-1}$. The impregnation, which lasted 12 hours, was carried out at room temperature in hermetically sealed jars and shaken for good homogenisation. After the 12 hours of impregnation, the material was filtered, then dried under study at 105°C for 24 hours in order to eliminate the interstitial and pellicular water content. Once dried, the material was carbonised for 3 hours at a temperature of 500°C in a SNOL oven in an oxygen-limited atmosphere. This phase creates pores in the material. The carbon was then characterised in order to highlight its physical and chemical properties. The activated carbon obtained is called BAN-K (Banana peel activated carbon with potassium hydroxide KOH).

Figure 1: Photography of banana peels during the drying period

2.1.3. Functionalization of activated carbon from MP

This phase consisted of attaching Iron nanoparticles to the activated carbon using Iron oxide (Fe_2O_3) powder. The iron oxide powder was purchased from Inoxia Ltd, (United Kingdom, 45 Dunsfold Park Cranleigh GU6 8TB). The preparation was done following an adaptation of the method used by Choudhury and Lansing (2021). To do this, a 5000-ppm iron oxide solution was prepared with distilled water. Then, the MP activated carbon was impregnated with the Fe_2O_3 solution at an impregnation ratio of 0.05 $g.mL^{-1}$ for 2.5 hours with stirring. The impregnated activated carbon was then filtered and dried in an oven for 12 hours at 110°C. The heterogeneous compound was placed in crucibles in oven at 300°C for 50 minutes under an inert atmosphere. This pyrolysis operation removes the bound water and attaches Fe^{2+} ions to the oxygen atoms belonging to the carbonyl or hydroxyl groups found on the surface of the activated carbon: this leads to the formation of the iron nanoparticles (Briton Bi, 2019). After this phase, the functionalized activated carbon was weighed before being ground to have a diameter distribution between 315 µm and 2 mm. This functionalized activated carbon was named BANK-Fe (Banana peel carbon activated with potassium hydroxide and functionalized with iron nanoparticles).

2.2. Characterization of activated carbon and functionalized activated carbon

2.2.1. Carbonization yield

The yield reflects the mass loss of the biomass during carbonisation. The mass (in grams) of the chars obtained was determined and the efficiency of the preparation was determined according to **Eqn. 1** (Kouadio et al., 2019):

$$R_c = \frac{m_c}{m_b}.100 \qquad \textbf{Eqn.1}$$

R_c *= carbonization yield (%), m_c: mass of coal (g), m_b: masse de biomass (g)*

2.2.2. Ash content

The ash content gives an indication of the inorganic, unusable part present in the coal. It is calculated using **Eqn. 2** (Koné et al., 2021):

$$T_c = \frac{m_3 - m_2}{m_1}.100 \qquad \textbf{Eqn. 2}$$

Tc *:* Ash content (%)**,** m1 : the mass of coal used (0.5 g), m_2 : the mass of the empty crucible before carbonization (g), m_3 : the mass of the filled crucible after carbonization (g)

2.2.3. pH of the activated carbon

To determine the pH of the different activated carbons (AC) BANK and BANK-Fe, a sample of 1.0 g of dry AC was added to 50 ml of demineralised water. The suspension was then stirred to equilibrium using a magnetic stirrer for 30 min and filtered. Finally, the pH of the solution was measured.

2.2.4. Scanning electron microscope analysis (SEM)

Scanning electron microscopy analysis was carried out using the HIROX SH-4000M. In order to have a good image resolution, the charcoal was metallized. In fact, a few grams of coal were introduced into the apparatus and the reading was done automatically.

2.2.5. Texture

The determination of the texture of the carbons was done by the adsorption of nitrogen at a temperature of 77 K. The specific surface was calculated using equation 44 of the Brunauer, Emmett and Teller (BET) theory (Brunauer et al., 1938) (**Eqn. 3**). For this purpose, a V-Sorb 2800 tool was used.

$$S_{BET} = \frac{V_m.N_A.a_m}{m.V_m} \qquad \textbf{Eqn.3}$$

S_{BET}: Specific surface area (m2/g), NA: Avogadro number, am indicates the surface area occupied by the N2 molecule (0.1627 nm^2 /molecule of nitrogen) m: mass of the sample (g) and VM: molar volume of N2 at TPN (22414cm^3/mol).

The total pore volume and pore distribution were determined by applying the Density Functional Theory (DFT) method.

2.2.6. Setting up an experimental design: full factorial design

The major interest of experimental designs lies in the fact that they make it possible to optimise the number of experiments to be carried out during the test phase, by determining the real factors or combinations of factors influencing the response of the system to be studied (Triboulet, 2008).

2.2.7. Selection of factors and responses for the full factorial design

The 3 factors (X_i) selected for the full factorial design study are 1-the moisture content in the AC, 2-biogas flow rate through the filter column, 3-the functionalization of AC (with or no without Fe_2O_3). Furthermore, the responses to be studied are the absorption capacity and the breakthrough time. They are noted Y_i.

2.2.8. Experimental domain

The experimental domain was constructed following the selected factors. It represents the space in which the factors can vary. The information drawn from the experimental results will only be valid within this domain. It is represented in **Table 1.**

Table 1: Experimental domain

Factors	Unit	Low level (-1)	High level (+1)
Water content in AC (X_1)	%w/w	0	25
Biogas flow rate (X_2)	$L.min^{-1}$	1	3
Impregnation with Fe_2O_3 (X_3)	-	Yes	No

2.2.9. Experimentation table

The translation of the experimental matrix into a directly usable matrix determining the different trials to be performed in the laboratory was carried out using the NEMRODW software. **Table 2** shows the different tests performed on experimental site.

Table 2: Experimental tests table

Tests	X_1	X_2	X_3	Y
Test 1	0	1	No	Y_1
Test 2	25	1	No	Y_2
Test 3	0	3	No	Y_3
Test 4	25	3	No	Y_4
Test 5	0	1	Yes	Y_5
Test 6	25	1	Yes	Y_6
Test 7	0	3	Yes	Y_7
Test 8	25	3	Yes	Y_8

2.2.10. Performing the adsorption tests

The different tests were carried out according to the previously established experimental design. The tests were carried out at the site of the Brin Foundation (an organisation owning poultry farms), in the sub-prefecture of Tabagne, in the north-east of Côte d'Ivoire where a 10 m^3 biodigester has been producing biogas continuously for several months. For the tests, two PVC filters of 10 cm height and 1.6 cm diameter, equipped with valves were designed. Fine pore fabrics were used on the filter to prevent the carbon from being entrained by the gas flow. These fabrics were also used as diffusers to allow a homogeneous distribution of the gas flow in the filter media. ACRYLIC flow meters of ±4% accuracy were used to regulate the gas flow at the filter inlet, to account for the values given in the experimental matrix. For each test, 5 g of carbon was used. 1.25 g of water (25% by mass) was weighed and added to the activated carbon or functionalized activated carbon for those tests where the X_2 variable was 25. The carbon and water were weighed in situ on a CONSTANT-14192-640C digital balance with an accuracy of ± 0.01 g. A series of measurements allowed us to fix the average H_2S content of the biogas at the filter inlet at 80 ppm : this value therefore represents the initial H_2S content (C_0) of the biogas. The C_0 value and the H_2S concentration at the filter outlet were measured as a function of time using a BOSEAN biogas analyser. All tests were performed at room temperature. **Figure 2** shows a sketch of the experimental protocole.

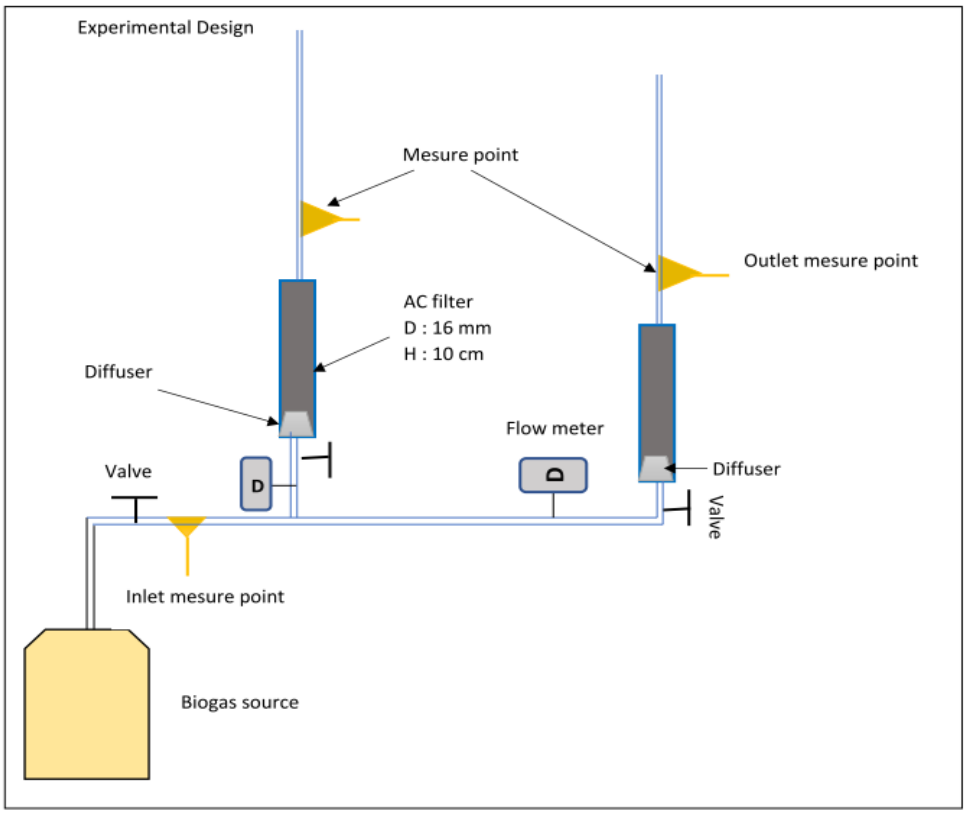

Figure 2: Sketch of the Experimental Pilot

The concentrations measured at the filter outlet as a function of time at each trial allowed the adsorption capacity $\mathbf{q_m}$ (mgH_2S/g material) to be calculated using **Eqn.4** (Choudhury and Lansing, 2021) and cited by Gbangbo et al. (2023):

$$q_m = \frac{Q.M}{m_c.V_m}.(C_e.T_s - \int_0^{T_s} C(t).dt) \qquad \textbf{Eqn. 4}$$

Where C_i is the concentration of H_2S at the filter outlet at time t_i

2.2.11. Expression of the mathematical model of the adsorption capacity

The mathematical expression is the mathematical model of a full factorial design for three factors (**Eqn. 5**):

$$qm(th) = b_0 + b_1X_1 + b_2X_2 + b_3X_3 + b_{12}X_1X_2 + b_{13}X_1X_3 + b_{23}X_2X_3 + b_{123}X_1X_2X_3 \qquad \textbf{Eqn. 5}$$

Where b_0 is the constant term in the regression equation; b_i is the coefficient associated with the factor X_i and b_{ij} is the coefficient associated with the interaction factor X_iX_j which reflects the interaction effect [26]. In the previous model, a coefficient is significant if its absolute value is greater than or equal to $2\sigma_e$. Where σ_e is the experimental error.

2.2.12. Main effects

The main effect of a factor reflects the action of that factor on the response when considered individually **Eqn. 6.**

$$E_{X_i} = \frac{1}{N}\sum_{i=1}^{N}(Z_{k_{X_i}}.Y_i) \qquad \textbf{Eqn. 6}$$

2.2.13. Effects of the 2nd order interactions

The second-order effects reflect the interactions between the factors in pairs (**Eqn. 7**):

$$E_{X_iX_j} = \frac{1}{N}\sum_{i=1}^{N}(Z_{k_{X_iX_j}}.Y_i) \qquad \textbf{Eqn. 7}$$

2.2.14. Effects of the 3rd order interactions

Third order effects reflect interactions between three factors taken together (**Eqn. 8**):

$$E_{X_iX_jX_m} = \frac{1}{N}\sum_{i=1}^{N}(Z_{k_{X_iX_jX_m}}.Y_i) \qquad \textbf{Eqn. 8}$$

In equations 6 to 8, N is the number of experiments (Yahiaoui, 2015)

2.2.15. Average of the responses

By definition, the arithmetic mean of a set of values is the sum of all values divided by the number of values (**Eqn. 9**):

$$\bar{Y} = \frac{1}{N}\sum_{i=1}^{N} Y_i \qquad \textbf{Eqn. 9}$$

Where N is the number of experiments (Yahiaoui, 2015).

2.2.16. Standard deviation

The definition of standard deviation is somewhat less straight forward than that of the mean. The standard deviation is defined as (Yahiaoui, 2015) (**Eqn. 10**) :

$$\rho^2 = \frac{1}{N-1}\sum_{i=1}^{N}(Y_i - \bar{Y})^2 \qquad \textbf{Eqn. 10}$$

2.2.17. Coefficient of determination (R^2)

The analysis of variance consists of looking for sources of variation in responses, assuming that the responses were calculated with the postulated model. The analysis of variance allows us to calculate a very useful statistic: the R^2 or R-squared (**Eqn. 11**). It allows us to know whether the model explains all of its results well by plotting the regression curve between the calculated responses and the experimental responses. This statistic is the ratio of the sum of the squares of the calculated (mean-corrected) responses to the sum of the measured (mean-corrected) responses (Yahiaoui, 2015):

$$R^2 = \frac{\sum_{i=1}^{N}(Ycal_i - \bar{Y})^2}{\sum_{i=1}^{N}(Yexp_i - \bar{Y})^2} \qquad \textbf{Eqn. 11}$$

The larger the R^2 and the closer it is to 1, the better the model (the calculated responses are strongly correlated with the experimental responses). However, if the number of experiments is equal to the number of unknowns in the system, the coefficient of determination is always equal to 1. To avoid this, the adjusted correlation coefficient has been introduced. It is given by **Eqn. 12**:

$${R_a}^2 = \frac{N-1}{N-P}(1 - R^2) \qquad \textbf{Eqn. 12}$$

Where : number of trials, et P : number of independent coefficients (Yahiaoui, 2015).

2.2.18. Determination of the relative contribution of the factors

The relative contribution of the factors on the different responses can be calculated using **Eqn. 13** (Yahiaoui, 2015):

$$P_i = \left(\frac{{b_i}^2}{\sum {b_i}^2}\right) \times 100\,, (i \neq 0) \qquad \textbf{Eqn.13}$$

Where P_i : relative contribution of factors and interaction of factors

b_i : statistical coefficient of the different factors

2.2.19. Validation of the mathematical model

Validation consisted of assessing the fit of the theoretical yiels to the experimental adsorption capacity by the means of the coefficients of determination R^2 and R^2 ajusted.

3. Results and discussion

3.1.Characteristics of the adsorbents

Table 3 presents the physical and chemical characteristics of BAN-K and BANK-Fe ACs that were evaluated. The BAN-K and BANK-Fe activated carbons have iodine indices of 1408.59 $mg.g^{-1}$ and 1065.96 mg.g-1 respectively. These high iodine index values show that these two carbons are probalbly microporous. Indeed, several authors have shown that the iodine index is an indicator of microporosity (Koné et al., 2021, Siragi et al., 2017), Moreover, these values are higher than the index values found in recent works: by producing activated carbon from plantain stem, by chemical activation, Briton (2019) obtained an iodine index value of 927 $mg.g^{-1}$. Moreover, these values are much higher than the iodine indices of certain commercial activated carbons found on the market. For example, activated carbons F100, F200 and F300 marketed by the company CHEMVIRON CHARBON in Belgium have respective iodine indices of 838±13, 863±13 and 876±13 $mg.g^{-1}$ (Nko'o et al., 2016). However, this hypothesis must be confirmed by N_2 adsorption isotherms at 77 K and the Density Functional Theory (DFT) method. Finally, we notice the decrease of the iodine index by 24.32% after Fe_2O_3 impregnation. This can be explained by the occupation of part of the micropores by the Fe particles. Indeed, the Fe_2+ cation of radius 0.076 nm (König, 2005). According to the IUPAC (International Union of Pure and Applied Chemistry) classification, micropores have a diameter of less than 2 nm (White et al., 2009). This would therefore facilitate the occupation of certain micropores by iron nanoparticles; hence the decrease in the iodine index from 24.32% after impregnation with Fe_2O_3. Both ACs show a morphology where pores of different aspects can be distinguished (**Figure 3**). Compared to BAN-K, the BANK-Fe AC shows apparently partially occupied pores. This can be explained by a partial occupation of the pores by the Fe particles contained in the Fe_2O_3. The ash and moisture content of BAN-K activated carbon are low: 12% and 14% respectively. These values give it the characteristic of a good activated carbon. Indeed, an excessively high ash content (> 20%) reduces the activity of the carbon, its reactivation potential and can generate impurity leakage (mineral salts). On the other hand, a low ash content (≤ 20%) indicates that the biomass consists mainly of organic matter (Siragi et al., 2017). The spectrum and chemical element mapping of the BANK are shown in **Figure 4** and **Figure 5** respectively. On the other hand, the high oxygen content (45.39%) is a major asset for the fixation of Iron atoms contained in Fe_2O_3 which was used to functionalise BAN-K coal to obtain metal oxides. This justifies the reduction of the oxygen content in BANK-Fe AC (18.31%) (**Table 3**).

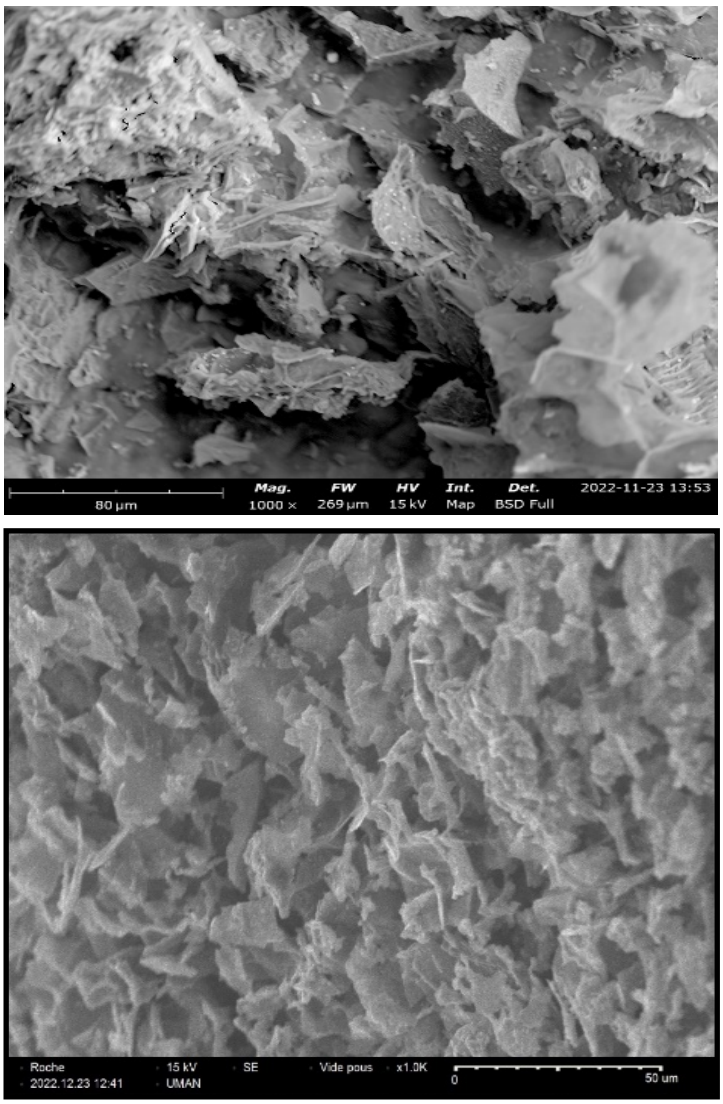

Figure 3. Morphology of charcoal seen by scanning electron microscope (SEM) : BAN-K (top); right) BANK-Fe (down)

Table 3. Physical and Chemical characteristics of BAN-K and BANK-Fe ACs

Parameters	Activated carbons	
	BAN-K	**BANK-Fe**
Carbonization efficiency (%)	34	27.83
Ash content (%)	12	12
Humidity (%)	14	14
Iodine value ($mg.g^{-1}$)	1408.59	1065.96
C (%)	57.01	62.25
O (%)	45.39	18.31
K (%)	0.21	10.86
Fe (%)	0.58	13.03
S (%)	0	0
Al (%)	0.68	15.75
Si (%)	0.68	1.05
Cu (%)	-	1.37
Ca (%)	0.27	-
Ph	9.981	9.672

The fixation of Fe atoms was effective: 13.03 % Fe was found on the BANK-Fe CA Fe and highlighted by the peak in **Figure 6**, against 0.58 % on the BAN-K CA, in other words, there is 22 times more Fe in the BANK-Fe than in the BAN-K.

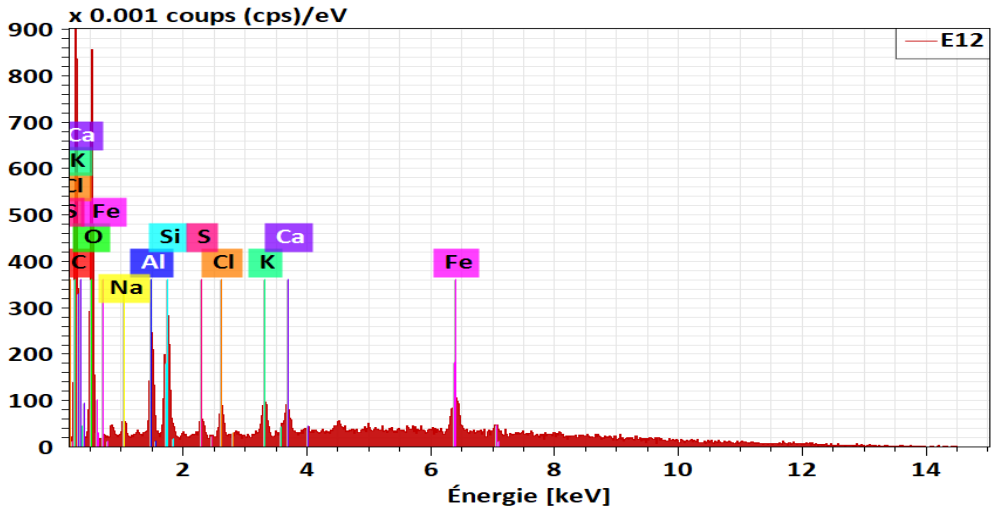

Figure 4. Spectrum of BAN-K using the BRUCKER EDS (Energy Dispersive X-Ray System)

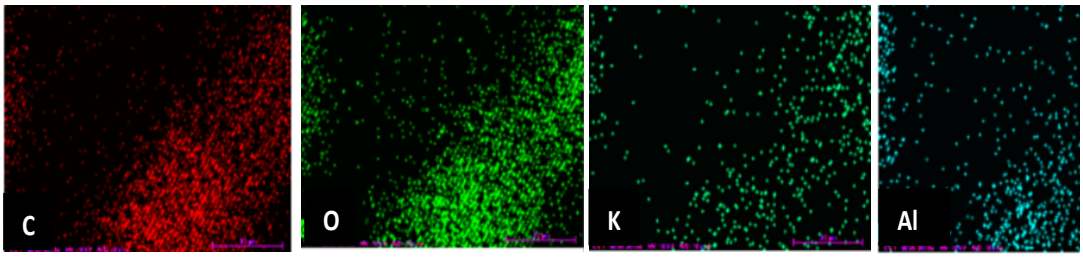

Figure 5. Spectrum and mapping of BAN-K at 20 µm

Figure 6 highlights the Fe peak found in the CA BANK-Fe. The hypothesis put forward in the previous paragraphs is therefore verified: the 24.32% reduction in microporosity and the change in the appearance of the surface morphology are due to the presence of Fe (**Figure 7**) after impregnation with Fe_2O_3. Furthermore, the potassium (K) elements probably come from the potassium hydroxide (KOH) that was used to carry out the chemical impregnation of the CA precursor. This type of observation has been made recently by certain authors: (Amadou and al., 2022) found phosphorus (P) elements in the matrix of chemical elements contained in the activated carbon that they produced by chemical activation with orthophosphoric acid (H_3PO_4).

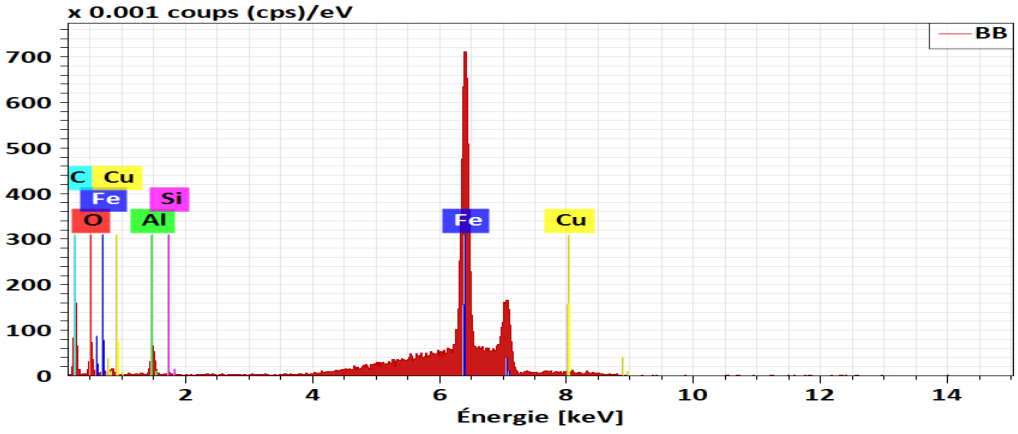

Figure 6. Spectrum of BANK-Fe using the BRUCKER EDS (Energy Dispersive X-Ray System)

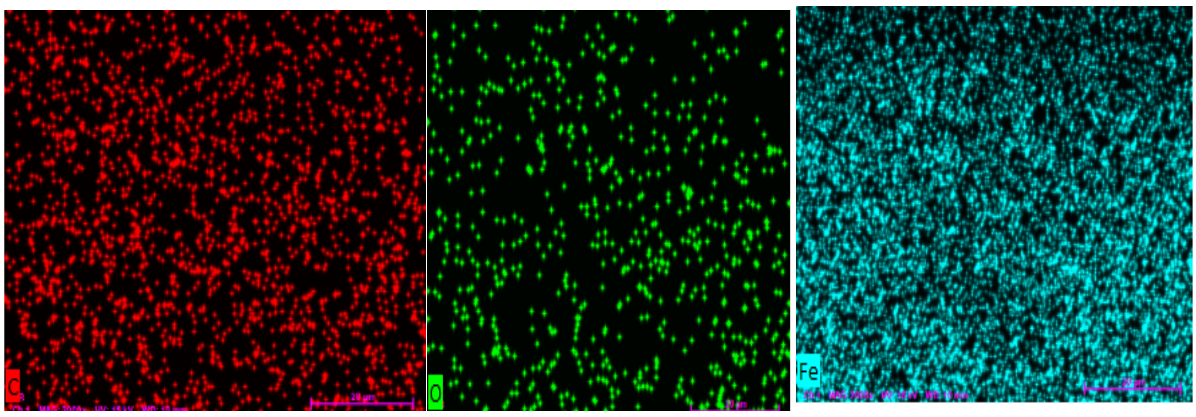

Figure 7. Chemical element mapping of BANK-Fe

3.2. Experimental adsorption capacities

The breakthrough curves of the H_2S adsorption tests on activated carbon under the different test conditions are shown graphically in **Figure 8**. The shortest and longest saturation times observed are respectively 17.6 minutes (test 3) and 615 minutes (test 6).

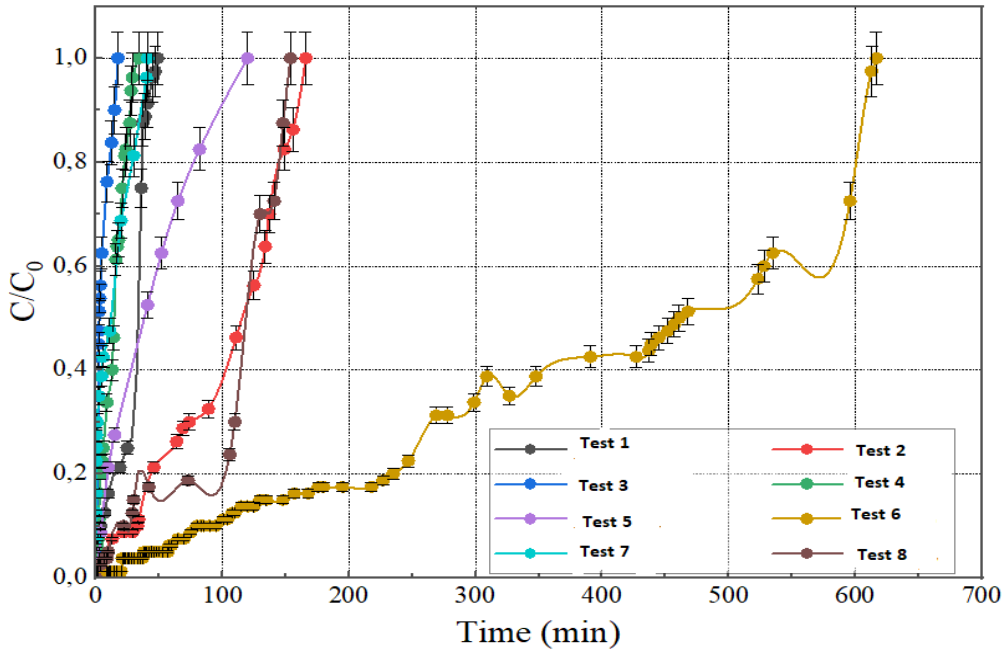

Figure 8. Adsorption curves of the different tests of the experimental matrix

The tests with a high biogas flow (3000 mL/min), without addition of water in the filter media, show shorter saturation times. Those with a low biogas flow (1 L/min) with a water content of 25% in the sorbent have relatively longer breakthrough times (Interval value). This is because at high flow rates, a large volume of biogas passes through the filter column in a relatively short time, so the amount of H_2S is proportionally high: this leads to rapid saturation of the activated carbon, as the contact time is low and does not favour the fixation of sulphur on the activated carbon. The opposite effect occurs at low flow rates. Furthermore, several studies have shown the positive influence of the presence of water on the surface of the activated carbon on the hydrogen sulphide adsorption mechanism. Indeed, when the materials used for H_2S adsorption contain water in their porosity, this favours the formation of an

aqueous film on the surface of the adsorbent. In the aqueous film, the H_2S molecules attached to the surface of the adsorbent can dissolve into their HS^- ionic form (Gasquet, 2021). This reaction saves the pore activity of the carbon and thus increases the saturation time. Furthermore, an exceptionally long saturation time is observed in test 6 where the biogas is passed at low flow rate over the activated carbon containing water is functionalised with contained iron nanoparticles. To better appreciate the efficiency of the activated carbon on H_2S adsorption under the different experimental conditions, the adsorption capacity at the different tests should be analysed. This parameter allows a better appreciation of the quantity of pollutants that can be retained by a unit mass of AC. The results of the adsorption tests are shown on **Figure 8.** The experimental response is the adsorption capacity of each of the eight (8) adsorption tests (**table 4**).

Table 4. Experimental adsorption capacities

Test	1	2	3	4	5	6	7	8	Standard deviation
qt ($mgH_2S.g^{-1}$)	0.67	2.49	0.4	1.04	1.08	9.86	1.03	7.83	0.1347

The adsorption capacities are strongly dependent on the experimental conditions which are, in this case, the previously defined factors: water content, Fe impregnation and flow rate. The main effects and interactions of these factors are described by the coefficients (**Table 5**) and the interaction diagram (**Figure 9**).

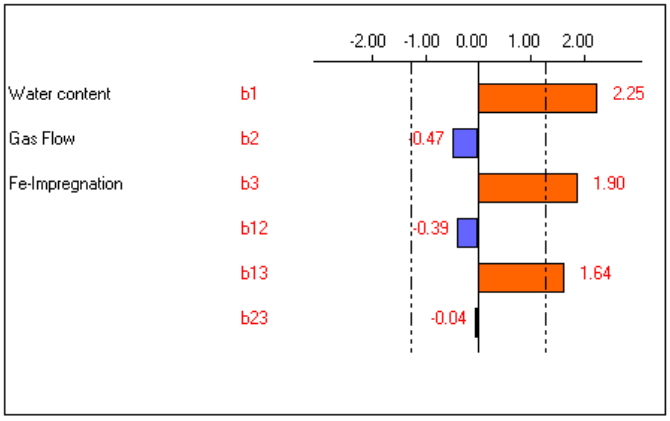

Figure 9. Diagram of interactions

3.3. Estimates and statistics of coefficients

The value of the experimental error obtained is σ_e= 0.1347. This value was used to determine which coefficients are significant and which are not. A coefficient is significant if its absolute value is greater than or equal to twice the experimental error $2\sigma_e$=0.2694. The different coefficients of the mathematical expression and their significance is shown in **Table 5.**

3.4. Expression of mathematical model

Taking into account only the significant coefficients, the model equation for the optimisation of hydrogen sulphide adsorption under the experimental conditions becomes (**Eqn. 14**) **:**

$$Y_{th}= 3.050 + 2.255X_1\text{-}0{,}475X_2 + 1.900X_3\text{-}0.395X_1X_2 + 1.640X_1X_3 \quad \textbf{Eqn. 14}$$

Table 5. Signification of coefficients

Name	Coefficient	Significance
b0	3.050	Significant
b1	2.255	Significant
b2	-0.475	Significant
b3	1.900	Significant
b12	-0.395	Significant
b13	1.640	Significant
b23	-0.045	Non Significant
b123	-0.10	Non Significant

The analysis of the coefficients through Table 7 allows us to understand the main effects and the effect of the interactions of the factors on the response. The coefficients b_1 and b_3 are positive: this means that in our experimental conditions, increasing the water content (X_1) and Fe impregnation (X_3) increases the adsorption capacity of the AC. The coefficient b_2 is negative: this means that when the flow rate is increased, the adsorption capacity decreases. Furthermore, there is an interaction between the 3 factors taken 2 by 2 because the coefficients b_{12}, b_{13}, b_{23} and b_{123} are non-zero. The negative sign of the coefficient b_{12} indicates that the water content and the increase in flow rate act simultaneously to reduce the adsorption capacity of the AC. In other words, if the water content in the AC filter medium is increased at the same time as the biogas flow rate through the filter is increased, the adsorption capacity of the AC is eventually reduced. This situation is shown in **Figure 10**. The positive sign of the coefficient b_{13} indicates that the water content and the iron impregnation act simultaneously in a positive way on the adsorption capacity: increasing the water content and at the same time impregnating the AC with Fe leads to a higher adsorption capacity of the AC, as shown in **Figure 10** and **Figure 11**.

The highest adsorption capacity of CA obtained under the experimental conditions is 9.86 $mgH_2S.g^{-1}$. It is obtained in test 6 with an addition of 25% water in the AC already impregnated with Fe. The biogas flow rate was 1 $L.min^{-1}$. The presence of water favours H_2S chemisorption through the formation of an aqueous film (Shang et al., 2016**)** and the Fe present in the solid allows to catalyse the H_2S dissociation and oxidation reactions through the following process (Gasquet, 2021): In a first step, metal sulphides (ferric sulphide taken here as an example) are formed. They are then oxidised by the oxygen present to form elemental sulphur and regenerate the metal oxides. The metal sulphides can also be further oxidised with organic or inorganic oxygen species, resulting in the formation of metal sulphates. The porosity of the best adsorbent (BANK-Fe) was evaluated. The determination of the pore volume volume and pore volume distribution of the AC is an important parameter to identify the type of pores on the surface (**Figure 12**). The micropore volume of AC BANK-Fe is 0.92 $cm^3.g^{-1}$. This value is ten times higher than 0.095 found by Choudhury and Lansing (2021). Previous work using activated carbons has shown that a high micropore volume, not necessarily a high surface area, results in a higher H_2S oxidation rate. This leads to a higher H_2S adsorption capacity (Choudhury and Lansing, 2021, Wallace et al., 2017).

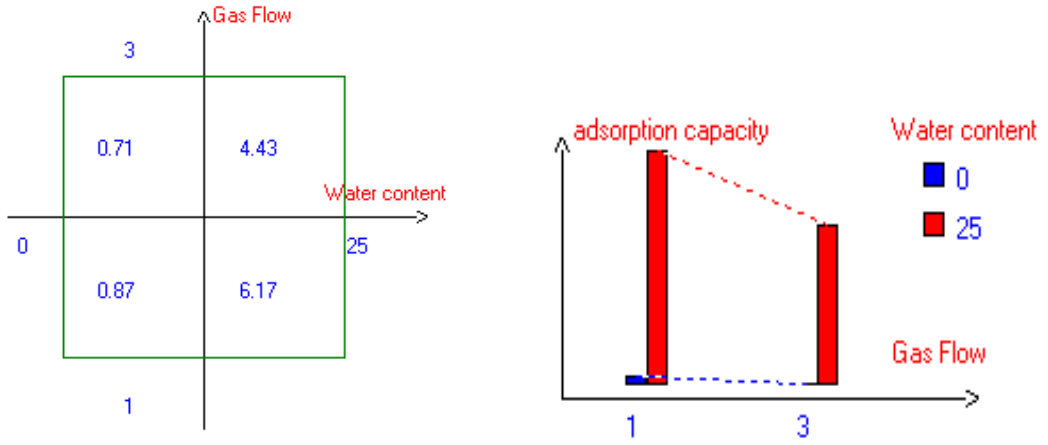

Figure 10. Combined effect of both water content and gas flow on adsorption capacity

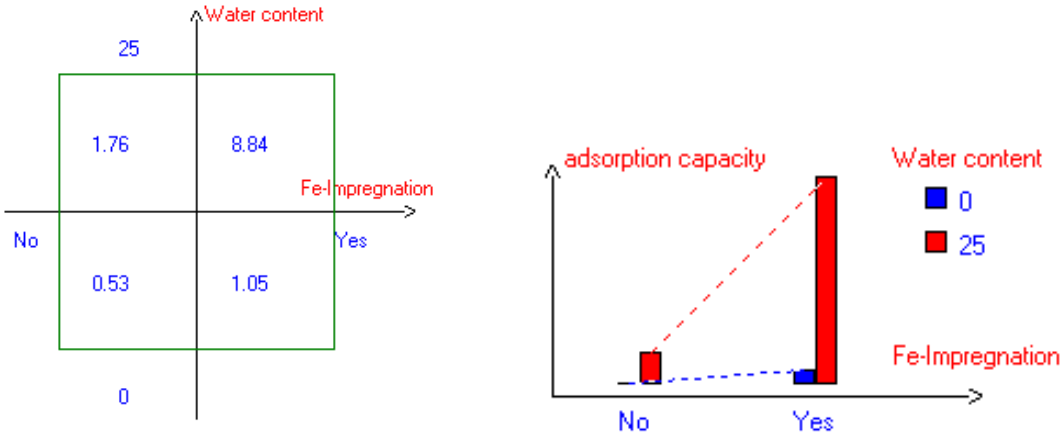

Figure 11. Combined effect of both water content and Fe-impregnation on adsorption capacity

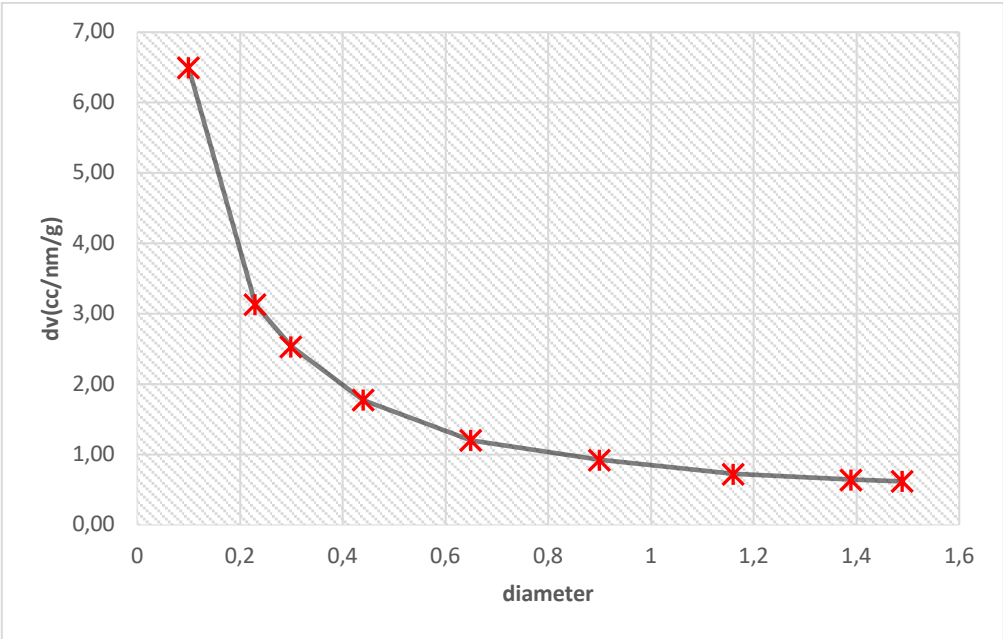

Figure 12. Pore distribution by DFT method

In addition to the pore volume, the 1.49 nm (**Table 6**) diameter obtained with the DFT method reflects the nanoporosity. Indeed, according to the IUPAC classification used by (Gueye, 2009) and (Melouki, 2022), pores smaller than 2 nm in diameter are called micropores; so the AC BANK-Fe contains micropores. Therefore, agreeing with (Alves et al., 2019) who reported that microporosity promote the movement of the adsorbate within the adsorbent resulting in better adsorption, it can be stated that BANK-Fe seems to be a better adsorbent compared to BAN-K. In addition, observation of the N_2 adsorption/desorption isotherm curve at 77 K (**Figure 13**) indicates a type IV isotherm. In accordance with the IUPAC classification, CA-BA contains micropores but remains more mesoporous. The prepared BANK-Fe gave a specific surface area of 76.18 m2/g (**Table 6**). This relatively low specific surface area is comparable to that found by Choudhury and Lansing (2021). They obtained a specific surface area of 59.8 m^2/g after impregnating an AC with an iron chloride solution.

Table 6. Morphological characteristics of CA BANK-Fe

Surface Area (m^2g^{-1})	Total pore volume ($cm^3.g^{-1}$)	Average pore width (nm)
76.18	0.92	1.49

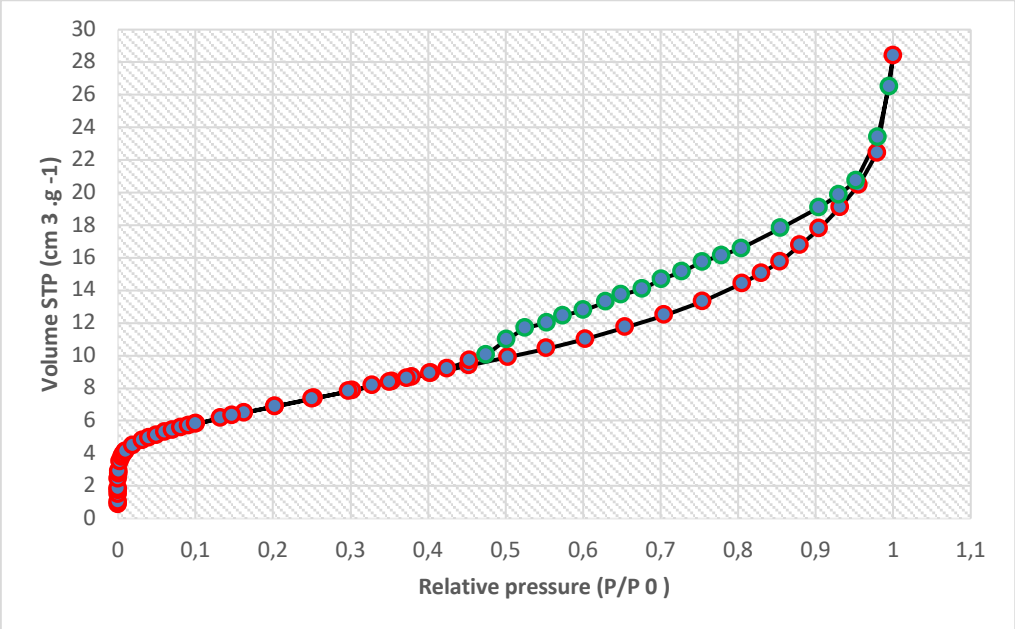

Figure 13. N_2 adsorption/desorption isotherm at 77 K (Red part: adsorption; green part: desorption)

Figure 14 shows a visual representation of the variation of the response as a function of the 2 parameters with the greatest impact on H_2S adsorption. The iso-response curves (**Figure 14**) allow a better appreciation of the evolution of the adsorption capacity of activated carbon as a function of water content and Fe nanoparticles. Moreover, the variance function (**Figure 15**) shows values between 0 and 0.05. This small value of the variance shows the relative constancy of the variation of the adsorption capacity as a function of the water content and the Fe content.

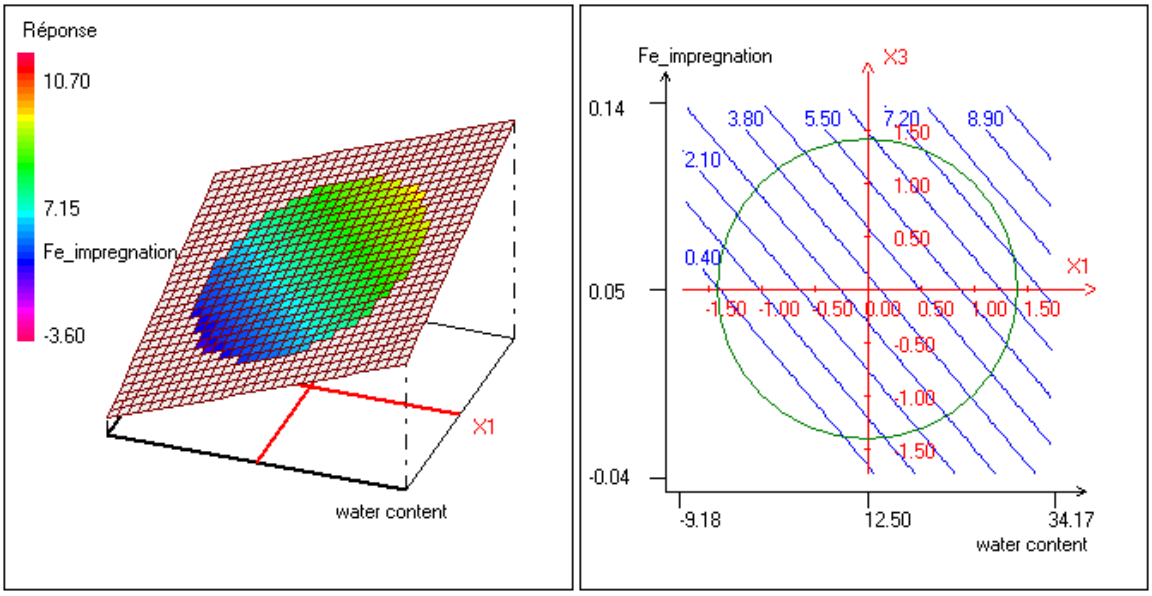

Figure 14. 2D and 3D isoresponses curves describing the variation of the response as a function of the factors X_1 and X_3

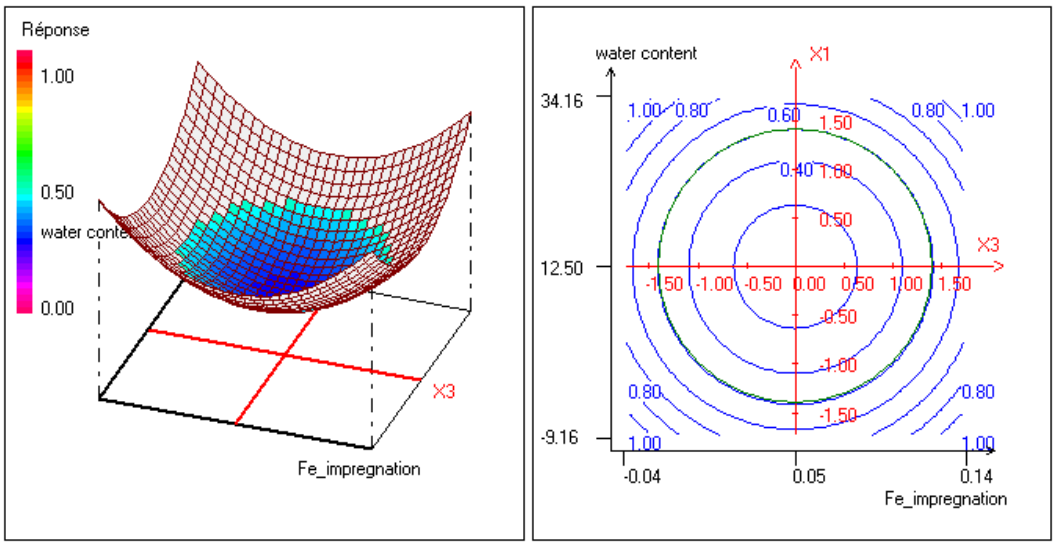

Figure 15. Variation of the variance function (Water content, Iron content)

3.5. Validation of the linear model of H_2S adsorption from biogas

The quality of the model is assessed through the coefficients of determination and the adjusted coefficient of determination (**Table 7**).

Table 7. Statistical Coeffiscients

Standard deviation of response	0.134
R^2	0.999
R^2 adjusted (R^2_a)	0.994

The R^2 value (0.999) allows us to conclude that the postulated model explains 99.99% of the studied phenomenon, while the remaining 0.01% is due to residuals. The R^2a value is 0.994, a value very close to unity, shows that the mathematical model is of good quality (Yahiaoui, 2015). In other words, the postulated mathematical model translates well the adsorption mechanism involved: the experimental response predicted by the model is close to the experimental values except for the residuals. These residuals represent the part of the response that is not explained by the highlighted effects (Yahiaoui, 2015). For each trial, the corresponding residual is calculated by establishing the difference between the measured response and the theoretical response. These residuals have an average value of 3.93%. This can be considered negligible: the experimental values are well predicted by the model to within 5%.

Conclusion

The aim of this study was to show the evolution of the adsorption capacity of PM-based activated carbon as a function of different factors considered simultaneously. From the experimental matrix, we were able to show that there are indeed interaction effects between the biogas flow rate, the water content and the fixation of Iron nanoparticles on the AC. Under the experimental conditions implemented, the most important interaction is that between water content and the fixation of Iron nanoparticles: they act simultaneously in order to increase the adsorption capacity of the PM activated carbon. The mathematical model describing the variation of the adsorption capacity as a function of the predefined factors is a first-degree linear model. The highest adsorption capacity (9.81 mgH_2S.mg-1) is obtained by adding 25% water to the Fe nanoparticle functionalized MP AC when the biogas flow rate through the filter media is 1 L.min$^{-1.}$

The use of biogas in biomethane installations is based on a certain required flow rate. This flow rate depends on the demand. Once this flow rate is known, stakeholders can improve the H2S adsorption process of the biogas by adding water to activated carbon and functionalized with iron nanoparticles. Both of these factors promote the adsorption of H_2S from biogas. However, the results of this study depend on the experimental range chosen for each factor: further studies can be carried out by extending the experimental range (range of values of each parameter) and see the possible evolution of H_2S adsorption from biogas.

Acknowledgments

The authors would like to thank Mr. Tchalimé PIDIMON-ESSOWERO (France) for his help in writing and data analysis via softwares. The authors would like to thank the management of CEA-VALOPRO (African Centre of Excellence for Waste to High Value Products, World Bank) for the student interns who were made available to us for this project. We also thank Mr. Nassirou AMADOU who helped us find laboratories for the analyses as well as the transport of the samples. Finally, We thank Mr. Dennis Tala and Mr. Kadio Isaac for the resources provided.

References

Abdirakhimov M., Al-Rashed M.H., Wójcik J. (2022). Recent Attempts on the Removal of H2S from Various Gas Mixtures Using Zeolites and Waste-Based Adsorbents. *Energies* 15, 5391. https://doi.org/10.3390/en15155391

Alves A.A. de A., Ruiz G.L. de O., Müller L.C., Sens M.L., Nonato T.C.M. (2019). Performance of the fixed-bed of granular activated carbon for the removal of pesticides from water supply. *Environmental technology* 40, 1977–1987.

Amadou K.M.N., al., (2022). Process conditions optimization of plant waste-derived microporous activated carbon using a full factorial design and genetic algorithm. *Journal of Materials and Environmental Science* 13, Page 884-899.

Awe O., Zhao Y., Nzihou A. (2017). A review of biogas utilisation, purification and upgrading technologies. *Waste Biomass Valorization.* 8, 267-283.

Briton Bi G.H., (2019). Elaboration de catalyseurs à base de nanoparticules de fer supportées sur du charbon actif pour le traitement des eaux usées textiles par le procédé fenton hétérogène. Institut National Polytechnique Félix Houphouet-Boigny, Yamoussoukro.

Brunauer S., Emmett P.H., Teller E. (1938). Adsorption of Gases in Multimolecular Layers. *J. Am. Chem. Soc*. 60, 309–319. https://doi.org/10.1021/ja01269a023

Choudhury A., Lansing S. (2021). Adsorption of hydrogen sulfide in biogas using a novel iron-impregnated biochar scrubbing system. *Journal of Environmental Chemical Engineering* 9, 104837. https://doi.org/10.1016/j.jece.2020.104837

Coffi J.P.-M., Lekadou T.T., Ama J.T., Traor S., Yao D.M.S., Agoh F.C., Koffi Z.E.B., Djaha E.K., Hala F.N. (2021). État des lieux des bananeraies (Musa sp.) en zone de culture du cocotier, sur le littoral en Côte d'Ivoire : cas de la station Marc DELORME et des villages aux alentours. *Int. J. Biol. Chem. Sci.* 15(6), 2438-2455,

Fougerit V. (2017). Développement d'un procédé innovant d'épuration du biogaz par mise en oeuvre de contacteurs à membranes. Université Paris-Saclay, Paris.

Gasquet V., (2021). Epuration d'H_2S du biogaz à partir de résidus de traitement thermique bruts et formulés : Comparaison des performances et compréhension des mécanismes d'adsorption.

Gbangbo K. R., Kouakou A. R., Ehouman A. D., Yao B., Goli Lou G. V.-E., Gnaboa Z., Bailly G. C. (2023). Influence of Water Content on Hydrogen Sulfide Adsorption in Biogas Purification with Musa Paradisiaca Biochar. *Chemistry Africa*, 6, 657–665 https://doi.org/10.1007/s42250-023-00610-w

Gueye, M. (2009). Synthèse et étude des charbons actif pour le traitement des eaux usées d'une tannerie.

Guterres A. (2022). Le monde brûle. Il nous faut engager une révolution fondée sur les énergies renouvelables, in: Groupe des Nations Unies pour le développement durable. Presented at the Conférence des Nations Unies sur les océans, United Nations, Potugal.

Insee (2022). La flambée des prix de l'énergie : un effet sur l'inflation réduit de moitié par le «bouclier tarifaire». Institut national de la statistique et des études économiques.

Juntarachat N., Onthong U. (2022). Removal of hydrogen sulfide from biogas using banana peel and banana empty fruit bunch biochars as alternative adsorbents. *Biomass Conv. Bioref.* https://doi.org/10.1007/s13399-022-03430-z

Koné, H., Assémian A.S., Tiho T., Adouby K., Yao K.B., Drogui P. (2021). *Borassus aethiopum* activated carbon prepared for nitrate ions removal. Journal of Applied Water Engineering and Research 10, 64–77. https://doi.org/10.1080/23249676.2021.1947400

König C. (2005). Chimie du fer : l'élément métal [WWW Document]. Futura Sciences. URL https://www.futura-sciences.com/sciences/dossiers/chimie-fer-tombe-masque-565/page/2/ (accessed 12.23.22).

Kouadio L.D., Koffi C.L.A., Diarra M., Kouyaté A., Yapi H.A.Y., Akessé V.P.D., Doungui B.K.D., Kone M., Dembélé A., Traoré K.S. (2019). Préparation et caractérisation de charbon actif issu de la coque de cacao. *Int. J. Adv. Res.* 7(6), 920-930

Melouki S. (2022). Synthèse, caractérisation de charbons actifs fonctionnalisés et étude de leurs applications en élimination de polluants. Université Mohamed Boudiaf de M'sila Faculté des sciences, Département de chimie.

Nabais J., Laginhas C., Carrott P. (2011). Production of activated carbons from almond shell. *Fuel Process Technol.* 92, 234-240.

Ngakou S.C. (2019). Optimisation de la préparation des charbons actifs par la Méthodologie des Surfaces de Réponse : Application à l'adsorption de la phénacétine en solution aqueuse, Dschang School of Sciences and Technology, Cameroune.

Nko'o A.M.C., Avom J., Mpon R. (2016). Évaluation des propriétés de charbons actifs de résidus de Moabi (Baillonella toxisperma Pierre) par adsorption d'iode en solution aqueuse. *Revue des Sciences de l'Eau,* 29, 51–60. https://doi.org/10.7202/1035716ar

Nyamukamba P., Mukumba P., Chikukwa E.S., Makaka G. (2022). Hydrogen Sulphide Removal from Biogas: A Review of The Upgrading Techniques and Mechanisms Involved. *International Journal of Renewable Energy Research*, 12, 557-568

Sawalha H., Maghalseh M., Qutaina J., Junaidi K., Rene E.R. (2020). Removal of hydrogen sulfide from biogas using activated carbon synthesized from different locally available biomass wastes - a case study from Palestine. *Bioengineered* 11, 607–618. https://doi.org/10.1080/21655979.2020.1768736

Sethupathi S., Zhang M., Rajapaksha A., Lee S., Mohamad Nor N., Mohamed A., Al-Wabel M., Lee S., Ok Y., (2017). Biochars as Potential Adsorbers of CH_4, CO_2 and H_2S. *Sustainability* 9, 121. https://doi.org/10.3390/su9010121

Shang G., Li Q., Liu L., Chen P., Huang X. (2016). Adsorption of hydrogen sulfide by biochars derived from pyrolysis of different agricultural/forestry wastes. *Journal of the Air & Waste Management Association* 66, 8–16. https://doi.org/10.1080/10962247.2015.1094429

Siragi D.B.M., Halidou I.H., Maman M.M.A., Zanguina A., Ibrahim N. (2017)). Elimination du chrome par du charbon actif élaboré et caractérisé à partir de la coque du noyau de Balanites Aegyptiaca. *Int. J. Biol. Chem. Sci.* 11, 3050-3065.

Sitthikhankaew R., Chadwick D., Assabumrungrat S., Laosiripojana N. (2014). Effects of humidity, O_2, and CO_2 on H_2S adsorption onto upgraded and KOH impregnated activated carbons. *Fuel Processing Technology* 124, 249–257. https://doi.org/10.1016/j.fuproc.2014.03.010

Triboulet P., 2008. Notions de bases sur les plans d'experiences.

UNEP, 2022. Données sur l'urgence climatique. United Nation.

Wallace, R., Suresh, S., Fini, E., Bandosz T., (2017). Efficient Air Desulfurization Catalysts Derived from Pig Manure *Liquefaction Char.* C 3, 37. https://doi.org/10.3390/c3040037

White R.J., Budarin V., Luque R., Clark, J.H., Macquarrie, D.J., (2009). Tuneable porous carbonaceous materials from renewable resources. *Chem. Soc. Rev.* 38, 3401. https://doi.org/10.1039/b822668g

World bank, (2022). Commodity Markets Oulook: The Impact of the War in Ukraine on Commodity Markets. WORLD BANK GROUP.

Yahiaoui I. (2015). Les plans d'expérience, initiation à la construction et à l'analyse des plans factoriels complets à deux niveaux et du plan central composite, *Université A. MIRA - Bejaia Faculté de Technologie Département de Génie des Procédés*.

Yuan J., Du L., Li S. (2019). Use of mature compost as filter media and the effect of packing depth on hydrogen sulfide removal from composting exhaust gases by biofiltration. *Environ Sci Pollut Res.* 26, 3762-3770.